Ultrasound Transmission Tomography Imaging of Structure of Breast Elastography Phantom Compared to US, CT and MRI

Krzysztof J. OPIELIŃSKI[(1)], Piotr PRUCHNICKI[(1)], Tadeusz GUDRA[(1)],
Przemysław PODGÓRSKI[(2)], Tomasz KRAŚNICKI[(2)], Jacek KURCZ[(2)], Marek SĄSIADEK[(2)]

[(1)] *Chair of Acoustics and Multimedia, Faculty of Electronics, Wrocław University of Technology*
Wybrzeże Wyspiańskiego 27, 50-370 Wrocław, Poland; e-mail: krzysztof.opielinski@pwr.wroc.pl

[(2)] *Department of Radiology, Wrocław Medical University*
Borowska 213, 50-556 Wrocław, Poland

The paper presents an analysis of the results of ultrasound transmission tomography (UTT) imaging of the internal structure of a breast elastography phantom used for biopsy training, and compares them with the results of CT, MRI and, conventional US imaging; the results of the phantom examination were the basis for the analysis of UTT method resolution. The obtained UTT, CT and MRI images of the CIRS Model 059 breast phantom structure show comparable (in the context of size and location) heterogeneities inside it. The UTT image of distribution of the ultrasound velocity clearly demonstrates continuous changes of density. The UTT image of derivative of attenuation coefficient in relation to frequency is better for visualising sharp edges, and the UTT image of the distribution of attenuation coefficient visualises continuous and stepped changes in an indirect way. The inclusions visualized by CT have sharply delineated edges but are hardly distinguishable from the phantom gel background even with increased image contrast. MRI images of the studied phantom relatively clearly show inclusions in the structure. Ultrasonography images do not show any diversification of the structure of the phantom. The obtained examination results indicate that, if the scanning process is accelerated, ultrasound transmission tomography method can be successfully used to detect and diagnose early breast malignant lesions. Ultrasonic transmission tomography imaging can be applied in medicine for diagnostic examination of women's breasts and similarly for X-ray computed tomography, while eliminating the need to expose patients to the harmful ionising radiation.

Keywords: ultrasound transmission tomography (UTT), ultrasonography (US), computed tomography (CT), magnetic resonance (MR) mammography, breast biopsy phantom.

1. Introduction

The unquestionable advantage of using ultrasound *in vivo* medical diagnostics is their harmless and non-invasive nature. Today, in the age of computerization, experts not only strive to perfect methods of ultrasonographic (reflection) imaging of tissue structure (NOWICKI, 2010; CAMACHO *et al.*, 2012; STOTZKA *et al.*, 2002), but also conduct intensive development of transmission methods (OPIELIŃSKI, 2011), focusing especially on ultrasonic projection UP (analogous to roentgenography RTG) (ERMERT *et al.*, 2000; OPIELIŃSKI, 2011; 2012; REGUIEG *et al.*, 2006) and ultrasound transmission tomography UTT (analogous to X-ray computed tomography CT) (DURIC *et al.*, 2007;

OPIELIŃSKI, GUDRA, 2010; OPIELIŃSKI, 2011; RUITER *et al.*, 2005).

The most common diagnostic tests used for early detection of breast malignant lesions include palpation, traditional X-ray mammography, ultrasound (US) imaging and MRI mammography (magnetic resonance imaging of women's breasts). Unfortunately, MRI cannot be performed in patients with cardiac pacemakers, neurostimulators, and ferromagnetic implants under any circumstances. Additionally, in patients with severe renal failure and/or allergy to contrast medium intravenous administration of contrast agents is contraindicated, which reduces the effectiveness of the examination. At a later stage cytological tests of biopsy-obtained material are performed.

There are also other diagnostic imaging modalities that can be implemented in prevention and diagnosis of breast cancer, such as (Opieliński, 2011): elastography (USE), thermography, electrical impedance tomography (EIT), single-photon emission computed tomography (SPECT), and positron emission tomography (PET). It became clear that ultrasound transmission tomography can also be used for imaging and early detection of breast malignant lesions (Duric *et al.*, 2007; Opieliński, 2011). Several research centres around the world (including the Chair of Acoustics and Multimedia of the Faculty of Electronics at Wroclaw University of Technology) are working to construct a prototype of UTT for women's breast examination (Duric *et al.*, 2007; Opieliński, Gudra, 2010; Opieliński, 2011; Ruiter *et al.*, 2005).

The following paper presents and analyses the results of ultrasound transmission tomography imaging of the internal structure of a CIRS Model 059 breast phantom used for ultrasonography (with elastography option) assisted biopsy training and compares them with the results of imaging by means of dual-energy CT method, MRI, and conventional US.

2. Materials and methods

A simplified block diagram of the research stand for UTT in divergent beam geometry with a constant angular distance, developed by the team at the Ultrasonic Technology Laboratory of Chair of Acoustics and Multimedia of the Faculty of Electronics at Wroclaw University of Technology is shown in Fig. 1 (Opieliński, 2011). The ultrasonic ring probe (Gudra, Opieliński, 2006) consists of 1024 of 0.5×18 mm piezoceramic sending-receiving transducers which are excited by short pulse signals with the frequency of 2 MHz and amplitude of 60 V_{pp} using a voltage amplifier and a demultiplexer system. Signals transmitted through the studied biological medium are received using a multiplexer and a receiving low noise
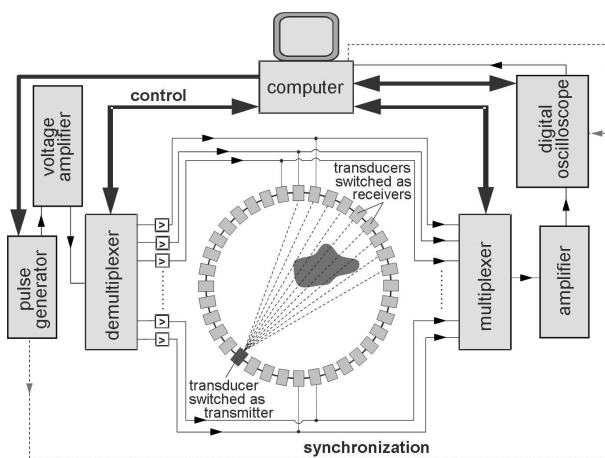

Fig. 1. Simplified block diagram of the measurement research stand for UTT with the ring probe.

amplifier. The received signals are registered by a computer using a digital oscilloscope card. The computer is then, by means of suitable software with acoustic parameter measurement algorithms, used to reconstruct images of a cross-section of the internal structure of the studied biological medium. One sending transducer and several hundred (usually 511) receiving transducers operate during one of the 1024 measurement cycles. The measurements are performed in distilled water that fills the ring probe tank, using a base, which allows precise vertical movement of the studied object.

A complete measurement of one cross-section, performed using the research stand, currently takes about 10 minutes. It will be reduced to a split of a second in the prototype by means of a parallel acquisition for each projection (the simultaneous recording of pulses from about 511 receiving transducers for each sending one), the FPGA based electronics, a faster transfer protocol, the parallel data processing, and the image reconstruction using CUDA^{TM} NVidia® graphic card with GPU's (graphics processing units). The reconstruction time using NVidia® is about few milliseconds for one cross-section image.

The CIRS Model 059 phantom mimics average values of acoustic parameters of tissues normal for the woman's breast for the purpose of elastography examination (Hoskins, 2010). The size (150:120:70 mm, volume: 600 cm^3) and shape of the phantom simulate female breast in the supine position. The phantom is made of Zerdine^{TM} gel, which imitates tissue and which contains 13 compact structure areas type inclusions that are about 3 times harder (rigid) than the surrounding gel. Those inclusions are positioned randomly inside the phantom. Inclusion size is in the range of about 2÷10 mm. One of the advantages of the phantom in relation to its use for transmission examination in water, is its smooth surface, which minimizes loss of oblique incident ultrasonic wave. It should be noted that according to the manufacturer, the inclusions in the phantom structure are not visible in images obtained using conventional ultrasonographs. They are, however, visible in elastograms (Hoskins, 2010). Average velocity of ultrasound in water was $c \approx 1490.6$ m/s ($t \approx 22.8$°C, temperature fluctuation $\Delta t \approx \pm 0.2$°C), in gel it was $c \approx 1503 \div 1507$ m/s, and in inclusions it was $c \approx 1510 \div 1515$ m/s.

The manner in which UTT examination of the phantom was performed is shown in Fig. 2. UTT images composed of 457×457 pixels with the size of 0.4 mm. Individual longitudinal cross-sections of the phantom (in the coronal plane – the base was perpendicular to the surface of the transducers) were measured with a vertical step of 2 mm, as shown in Fig. 3. The fast filtered back projection algorithm with Hamming filter assuming straight-line propagation was used for the image reconstruction (Kak, Slaney, 1988).
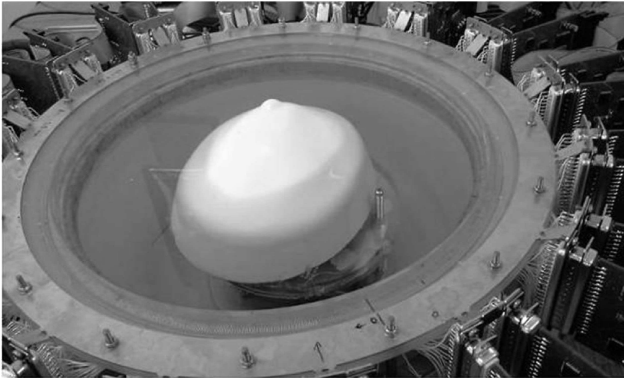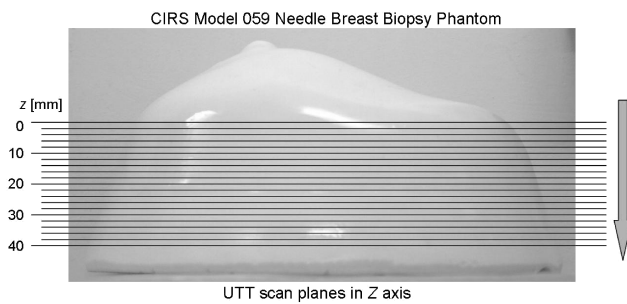
Fig. 2. Measurement UTT methodology.

Fig. 3. Way of UTT measurements of individual longitudinal cross-sections of the phantom.

The manner in which conventional US examination of the phantom was performed is shown in Fig. 4. The transversal cross-sections of the phantom were imaged using a 3.5 MHz and 5 MHz linear probe (operating with a Picker LS2400 scanner), that was submerged in water and moved along the phantom on a special base with a horizontal step of 5 mm.
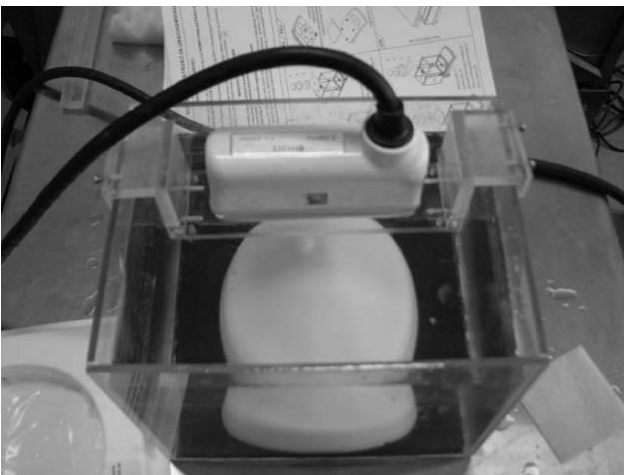

Fig. 4. US measurement methodology – a view of the tank.

CT and MRI examinations of the phantom were performed in the Department of General Radiology, Interventional Radiology and Neuroradiology of the Wroclaw Medical University Hospital, using Discovery

CT 750HD GE Healthcare and Signa HDxt 1.5T, GE Healthcare devices respectively (Fig. 5). The CT examination was performed using a dual-energy protocol: 80 keV and 140 keV (WANG, PELC, 2011). Next, secondary reconstructions of images for energy of 40 keV were obtained using dedicated software (GSI Viewer, GE Healthcare). The phantom was positioned so that its base was parallel to the surface of the gantry hole and perpendicular to the axis of the table surface (the coronal plane). The layer thickness was 0.625 mm and the resolution of the obtained image reconstructions was 512×512 pixels with the size of 0.52 mm. For the MRI examination the T2 FSE sequences were obtained using the following parameters: repetition time $T_r = 4940$ ms and echo time $T_e = 80.3$ ms. The phantom was examined using the 8-channel coil dedicated for breast imaging (8ch HD Breast Array). The phantom was positioned in a special breast grip, with the side surface parallel to the gantry hole. The layer thickness was 5 mm. The resulting array size was 512×512 pixels with the size of 0.38 mm.
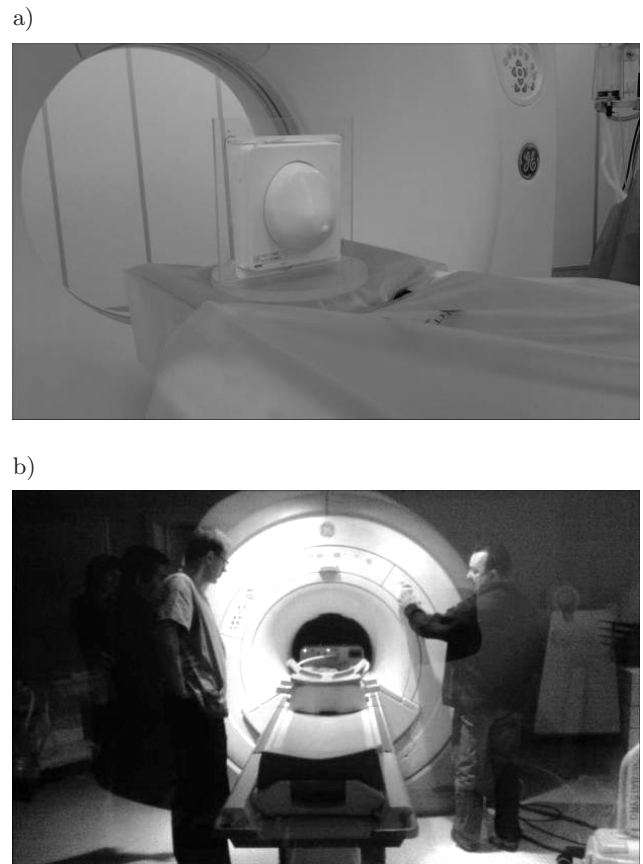
a)

b)

Fig. 5. Way of the breast phantom CT (a) and MRI (b) measurements.

3. Imaging

The results of UTT examinations for the longitudinal cross-section of the CIRS Model 059 phan-

a)   b)   c)

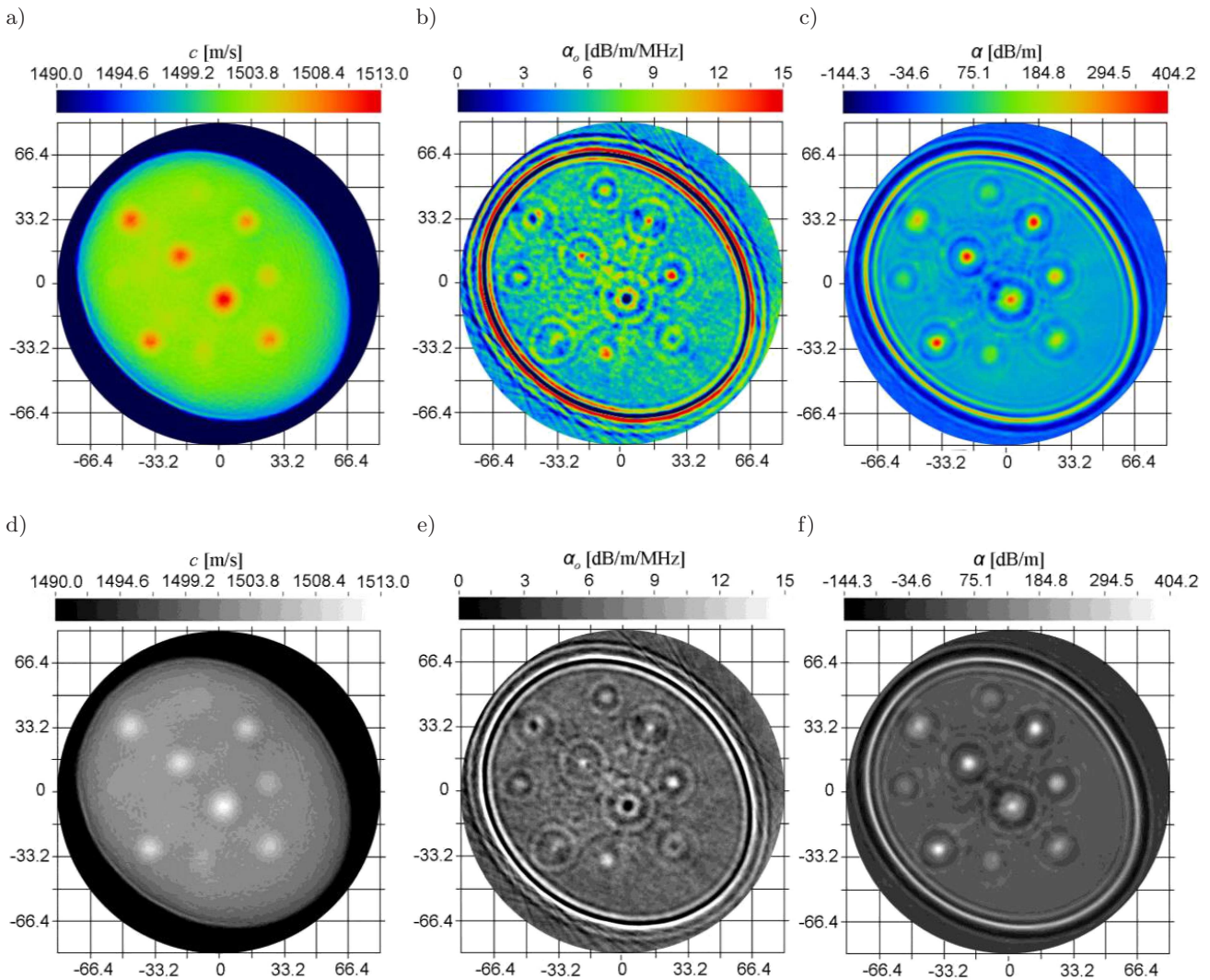d)   e)   f)

Fig. 6. UTT images of the CIRS Model 059 phantom longitudinal cross-section at the height of $z = 20$ mm (presented in rainbow colours and greyscale): a), d) ultrasound propagation velocity, b), e) derivative of the ultrasound attenuation coefficient in relation to frequency, c), f) the ultrasound attenuation coefficient.

tom (the coronal plane) for the selected height of $z = 20$ mm (see Fig. 3) are shown in Fig. 6. Three different UTT images in rainbow colours and greyscale from black to white (Fig. 6) were reconstructed from the determined values of ultrasonic pulse parameters recorded in the cross-section for divergent geometry (runtime, amplitude, frequency (DURIC *et al.*, 2007; OPIELIŃSKI, GUDRA, 2010; OPIELIŃSKI, 2011; 2012)). The images correspond in turn to distributions of local ultrasound velocity values, derivative of ultrasound attenuation coefficient in relation to the frequency and ultrasound attenuation coefficient (OPIELIŃSKI, GUDRA, 2010; OPIELIŃSKI, 2011; 2012). Negative and inflated values of the attenuation coefficient (Fig. 6c,f) result from errors of attenuation reconstruction based on the pulse amplitude – it is additionally reduced by phenomena occurring during ultrasonic wave transmission (OPIELIŃSKI, 2011). The most significant distur-

bances occur near the heterogeneity borders (signal loss and dropout). The images of the distribution of ultrasound attenuation derivative and ultrasound attenuation are significantly affected by multiple reflections with low amplitudes which cause so-called edge radiation (OPIELIŃSKI, 2011) (Fig. 6b,c,e,f).

Examples of US images of transversal cross-sections of the CIRS Model 059 phantom (where inclusions expected) obtained using a 3.5 MHz linear probe are shown in Fig. 7. The US scanning with a 5 MHz linear probe was inconvenient because the probe length was shorter than the phantom width, but none of the US images of the examined phantom cross-sections made it possible to see the heterogeneity of its structure.

The CT image of the CIRS Model 059 phantom longitudinal cross-section (in the coronal plane) for the height of $z = 20$ mm is shown in Fig. 8.
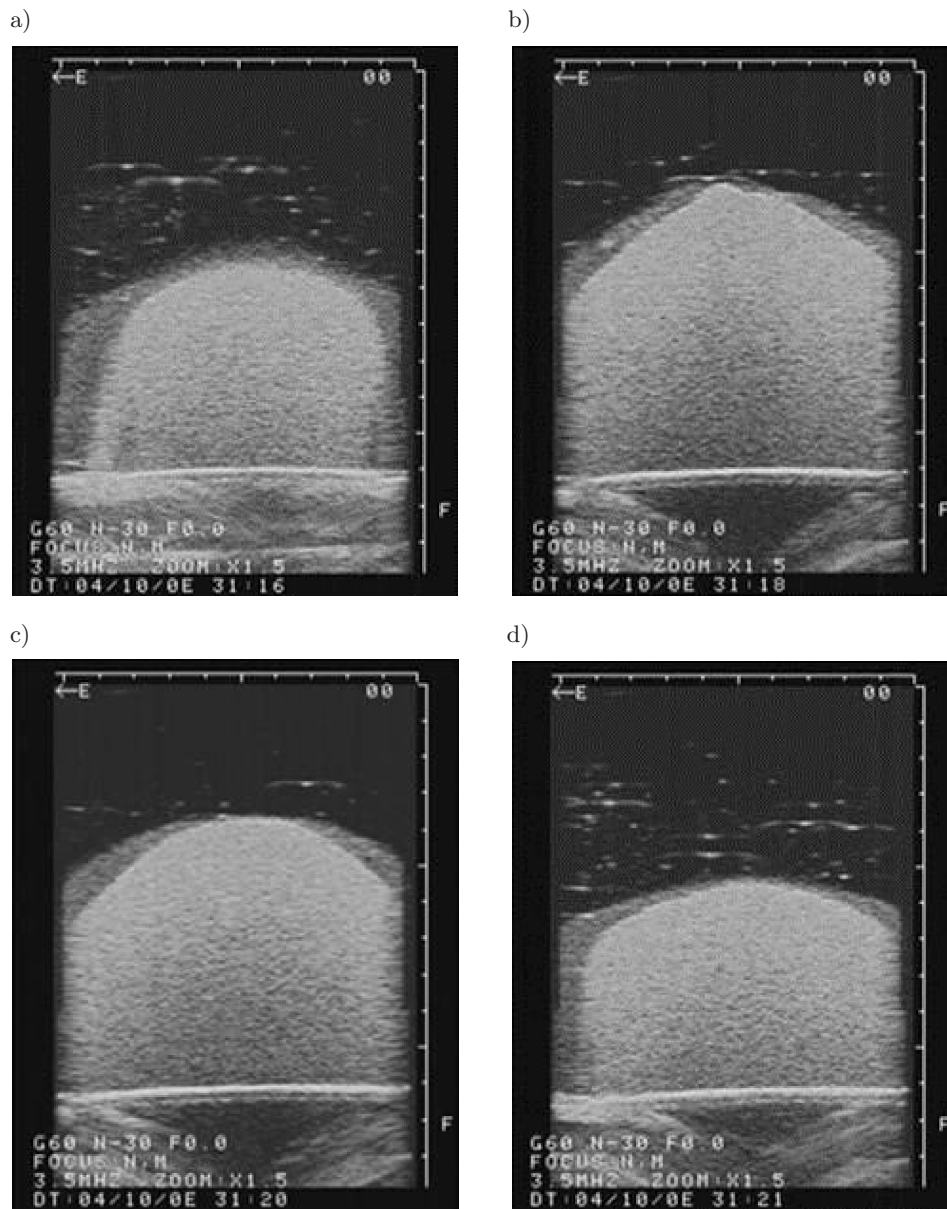
a) b)

c) d)

Fig. 7. Examples of US images of transverse cross-sections of the CIRS Model 059 phantom for the following distances of the linear probe axis from the edge of the tank (where inclusions expected): a) 2 cm, b) 5.5 cm, c) 7.5 cm, d) 11 cm.
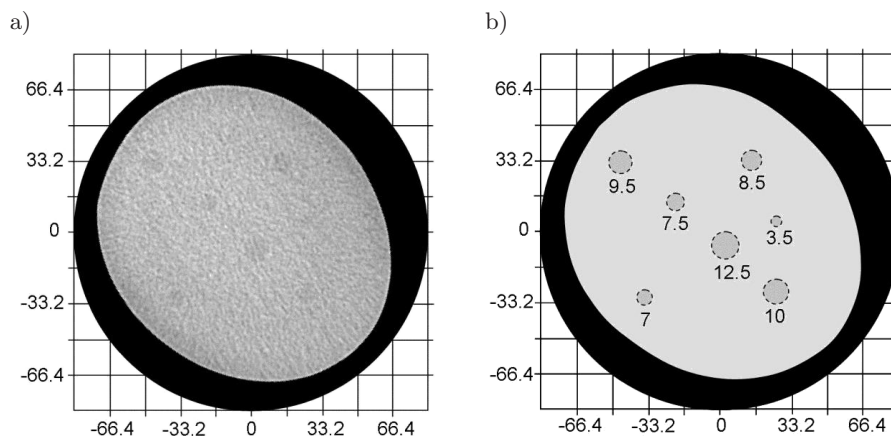
a) b)

Fig. 8. CT image of the CIRS Model 059 phantom longitudinal cross-section for the height of $z = 20$ mm: a) increased contrast image, b) estimation of the size of distinguishable heterogeneous areas using an edge rendering image method.
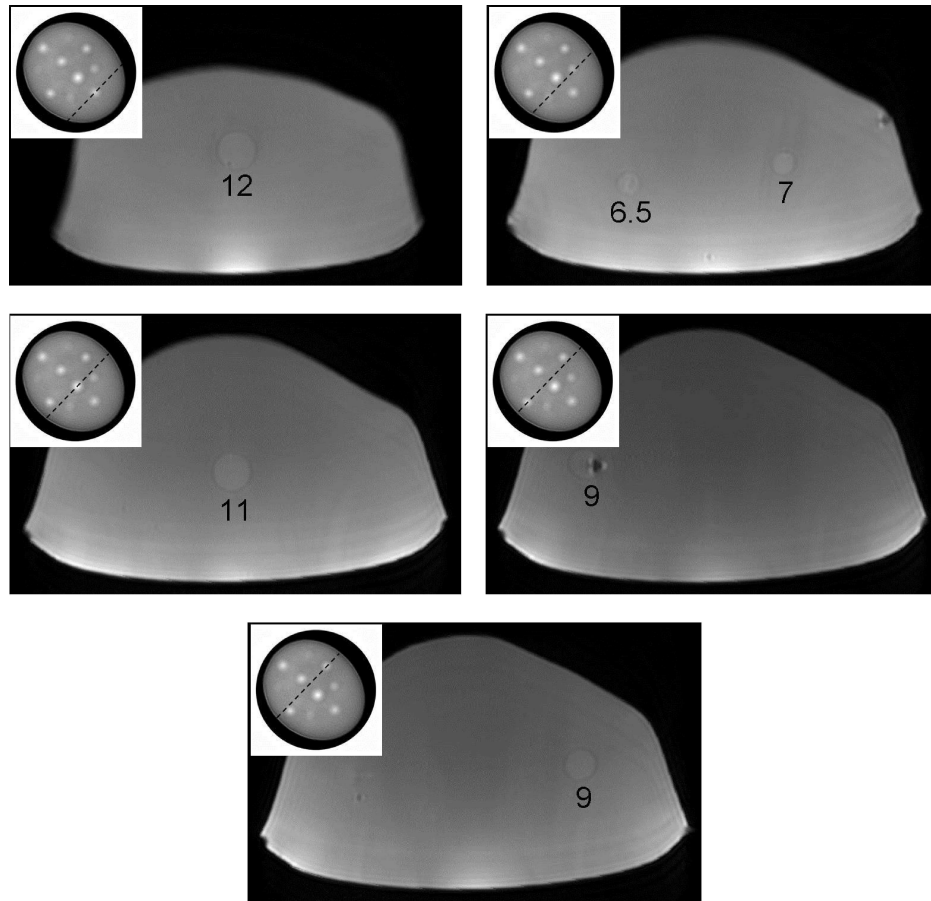
Fig. 9. MRI images of transverse cross-sections of the CIRS Model 059 phantom along selected heterogeneous areas which are presented on miniature UTT images (contrast was increased for better visibility of the inclusions).

Selected results of MRI examination of transversal cross-sections of the CIRS Model 059 phantom are shown in Fig. 9. For each MRI image the dashed line indicated the cross-section in relation to the UTT image of the ultrasound velocity distribution (Fig. 6d), and the size of the imaged heterogeneous areas was determined.

4. Image analysis

4.1. Computed Tomography

Breast tomosynthesis (3D mammography) is an adequate method for 3D breast imaging, however, in order to retain the shape and structure of the phantom used in this study, CT method was implemented. The CT method is not typically used in diagnostic management of the women's breast because of high kV values (usually 120 kV) used, which leads to a low diversity of tissue radiation attenuation. For the same reason, CT images of the CIRS Model 059 breast phantom structure reconstructed from direct measurements using energy of 80 keV or 140 keV, did not allow to recognize heterogeneous areas. However, inclusions in the phantom gel could be visualised on secondary reconstruction images obtained in dual-energy CT examination at the virtual energy level of 40 keV (Wang, Pelc, 2011). The visualised inclusions have sharply delineated edges but are hardly distinguishable from the phantom gel background (the contrast values between structures and the background contain in the maximum range 0÷6 dB and the average value is about 3 dB, see Table 1) even with increased image contrast (Fig. 8a). In a standard CT examination, radiological density (the level of X-ray opacity) and Hounsfield scale (based on radiological density), which is a linear transformation of the original linear attenuation coefficient measurement for X-rays, are the differentiating parameters. The darker areas are called hypodense, whereas the brighter ones are hyperdense. Radiodensity of distilled water in standard temperature and pressure is defined as zero on Hounsfield scale, while air density in typical conditions is −1000 Hounsfield units (HU) (Pruszyński, 2000). Multi-energy imaging modality utilises evaluation based on the measurement of relative atomic number of the examined tissues. The value of beam's linear attenuation coefficient for two different energies is simultaneously tested in

dual-energy CT imaging. The linear attenuation coefficient is dependent on two phenomena occurring during radiation-matter interaction: Compton scatter and photoelectric effect. These phenomena depend on the substances radiation interacts with. Therefore, it is possible to measure the distribution of the effective atomic number in the examined tissues. Next, based on the linear attenuation coefficient value one can calculate HU values of the tested material for specified energy.

The CT method is characterised by soft tissue contrast resolution of about 0.2%. Potential spatial resolutions achievable in CT systems are about 0.2÷0.3 mm (Pruszyński, 2000), which is why CT images of the structure of the examined phantom became the comparative standard and were the basis when calculating the size of the visualised heterogeneous areas (Fig. 8b).

4.2. Ultrasound Transmission Tomography

Figure 10a shows (in rainbow colours) an UTT image of the distribution of local values of propagation velocity of ultrasonic wave for the CIRS Model 059 phantom longitudinal cross-section for the height of $z = 20$ mm, with contours of the shape of the phantom longitudinal cross-section and inclusion edges rendered from a CT image for the same cross-section (Fig. 8b) by means of an edge detection algorithm using the Laplace image filter (Watkins *et al.*, 1993). In order to sharpen inclusion edges, Fig. 10b shows the same image in greyscale with suitably boosted contrast (50 → 80%) and reduced brightness (50 → 32%). Figure 10a and Fig. 10b also show lines of image pixels, the value distribution of which was drawn in Fig. 11 for 3 different UTT images (see Fig. 6). Analysis of the graphs of pixel values along the diameters of individual phantom

inclusions demonstrates that the 3 visualised distributions of local values of acoustic parameters: the ultrasound velocity c, derivative of the ultrasound attenuation coefficient in relation to frequency $\alpha_o = \partial\alpha/\partial f$, and ultrasound attenuation coefficient α are perfectly complementary to each other.

The image of ultrasound velocity (Fig. 6a,d) is a quantitative image, which makes it possible to distinguish heterogeneous areas from the background that differ in ultrasound velocity by at least one [m/s]. It is also possible to visualise both continuous and stepped changes (Fig. 6a,d shows water penetrating the edges of the phantom gel). One disadvantage of this type of imaging is fuzzy edges, which results in errors in evaluation of the size of inclusions and distorted ultrasound velocity values in small heterogeneous areas caused by multipath effect during ultrasonic wave propagation in a heterogeneous structure (Crawford, Kak, 1982).

Quan and Huang (2007) determined on the basis of simulation calculations that due to the multipath effect, ultrasonic transmission tomography based on runtime measurements (image of the distribution of ultrasound velocity) allows precise reconstruction of the ultrasound velocity for structures larger than 5 wavelengths. For structures smaller than 2 wavelengths, reconstruction is more qualitative, as it only makes it possible to identify heterogeneous areas, but distort local ultrasound velocity values inside.

Based on earlier research conducted by Opieliński and Gudra (2006) it can be concluded that in the case of real objects with diversified structure, the ability to visualise heterogeneous areas: their shape and velocity values in their internal structure, depends additionally on the actual value of the difference between the ultrasound velocity in a heterogeneous area and around it, on the effect of refraction, as well as on the lateral and
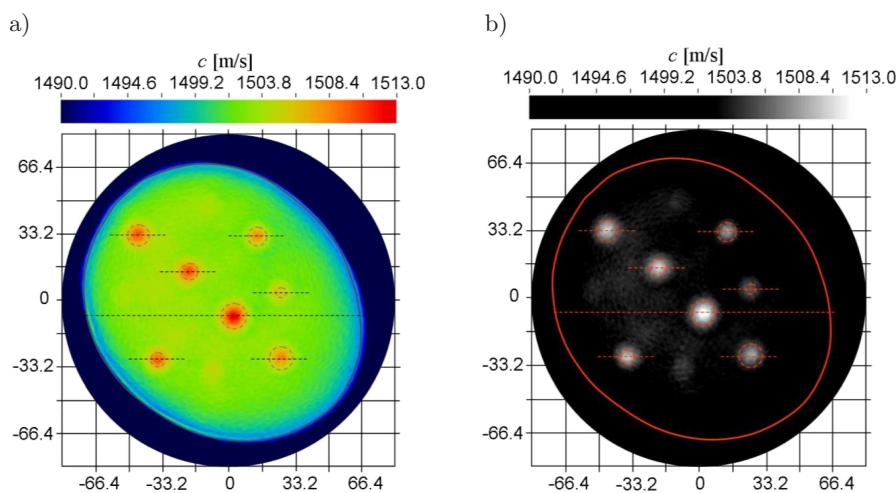

Fig. 10. UTT image of distribution of local values of ultrasound velocity for the CIRS Model 059 phantom longitudinal cross-section for the height of $z = 20$ mm, with contours of the shape of the cross-section and inclusion edges rendered from a CT image (Fig. 8b): a) rainbow colours image, b) greyscale image with boosted contrast (50 → 80%) and reduced brightness (50 → 32%).
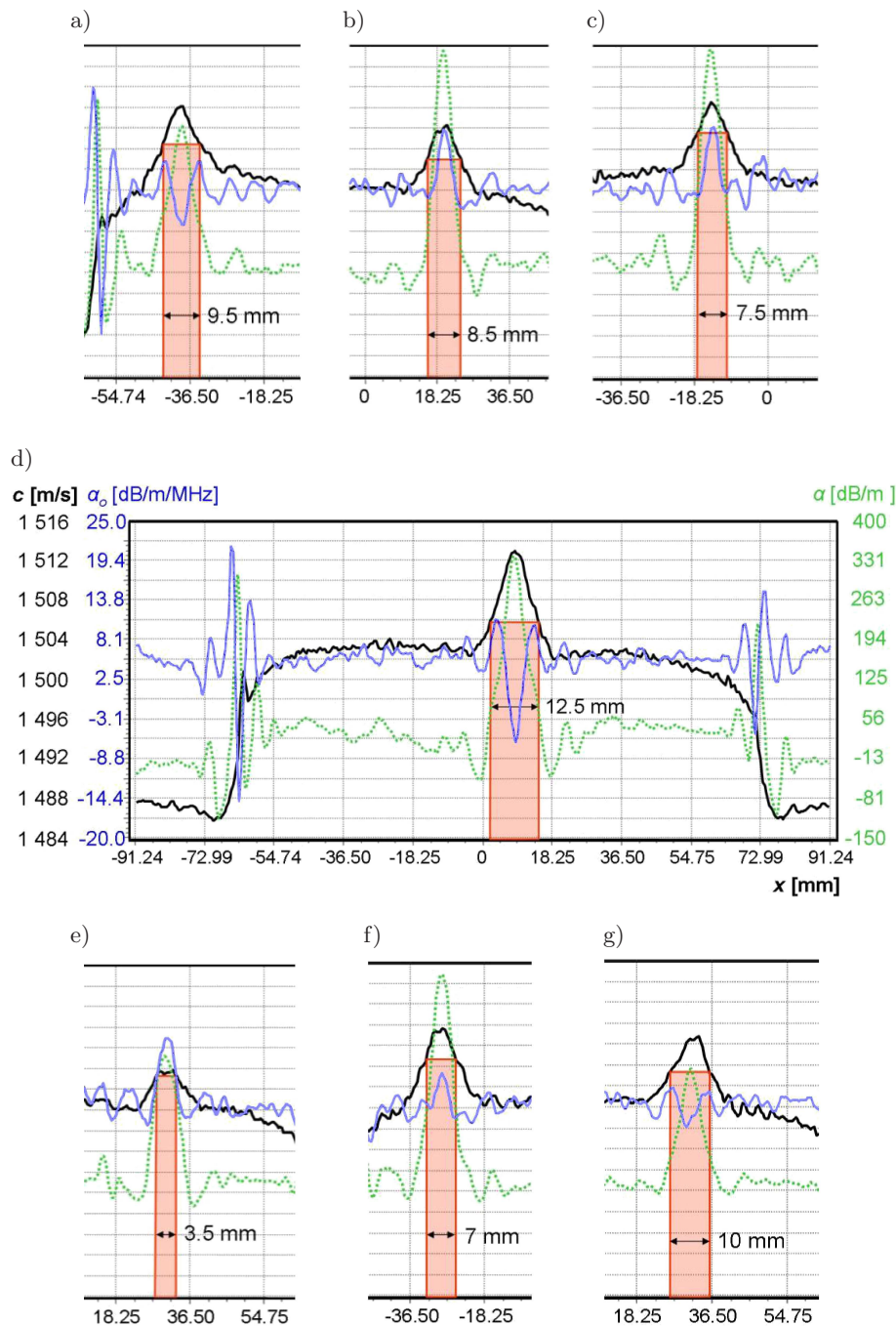
Fig. 11. Pixel value distributions for the lines indicated in Fig. 10, along the diameters of individual phantom inclusions, drawn in turn for 3 different UTT images (see Fig. 6), the ultrasound velocity – black colour, derivative of ultrasound attenuation coefficient in relation to frequency – blue colour, ultrasound attenuation coefficient – green colour: a) $d_{inc1} = 9.5$ mm, b) $d_{inc2} = 8.5$ mm, c) $d_{inc3} = 7.5$ mm, d) $d_{inc4} = 12.5$ mm, e) $d_{inc5} = 3.5$ mm, f) $d_{inc6} = 7$ mm, g) $d_{inc7} = 10$ mm.

longitudinal resolution. In the case of measurements of ultrasound velocity values by detection of the ultrasonic wave pulse runtime using digital methods, it is possible to determine the projection value of runtime with the precision of single nanoseconds. Therefore, projection value of the ultrasound velocity can be determined with the precision of about 0.01 m/s (when ignoring measurement uncertainty which can be much higher depending on the measurement setup and conditions, as well as noise and interference). This means that for the measured projection values of the ultrasound velocity it is possible to identify the influence of an inclusion for its size appropriately correlated with the difference between the local velocity value in the structure of this inclusion and the structure around it. If the existence of an inclusion alters projection values

of the ultrasound velocity measured from multiple directions, it will be possible to identify the inclusion in an UTT image reconstructed based on such measurements. Calculations show that if the total precision of determining projection values of the ultrasound velocity is at 0.01 m/s, it will be possible to distinguish, in an UTT image, heterogeneous areas different from the surrounding tissue in the value of the ultrasound velocity: 1 m/s with the size > 2.3 mm, 2 m/s with the size > 1.2 mm, 5 m/s with the size > 460 μm, 10 m/s with the size > 240 μm, 15 m/s with the size > 160 μm, 20 m/s with the size of 120 μm (Fig. 12). For any precision of determining projection values of the ultrasound velocity, UTT contrast resolution can be determined from graphs presented in specific papers (OPIELIŃSKI, GUDRA, 2006; OPIELIŃSKI, 2012).
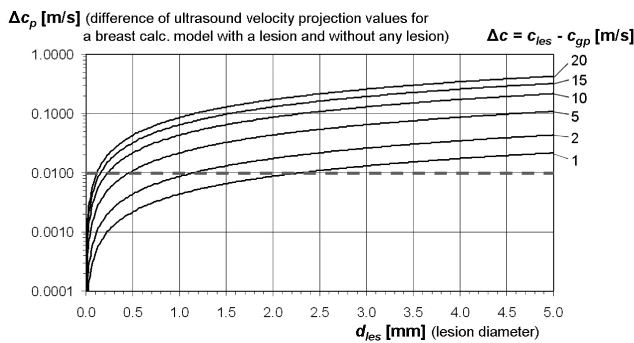

Fig. 12. Calculations of the difference of ultrasound velocity projection values for a breast calculation model with a lesion and without any lesion, depending on the lesion diameter, with the parameter $\Delta c = 1, 2, 5, 10, 15, 20$ m/s.

Moreover, a strict limitation is in effect related to longitudinal resolution dependent on wavelength and scanning pulse length. The calculated contrast resolution increases with decreasing relation between transmitter-receiver distance and inclusion size. Change of the ultrasound velocity in the coupling medium (water) surrounding the examined tissue has negligible influences (OPIELIŃSKI, 2012). Heterogeneous areas are usually diversified in terms of shapes and sizes. In such cases, the heterogeneous areas will be visible in projection measurements for some projection planes and not visible for others. Existence of such discontinuities will be visualised in a tomographic UTT image, if the difference of ultrasound velocity values in a projection (caused by structure heterogeneity in relation to the surroundings) are detectable for at least a few projection directions.

The image of derivative of the ultrasound attenuation coefficient in relation to frequency (Fig. 6b,e) is better for visualising edges but bad for continuous changes, in general. It is rather a qualitative image because it distorts the reconstructed absolute values as a result of received pulses being overlapped by side and multiple reflections and interference, as well as assuming linear changes of ultrasound attenuation with frequency in the process of reconstruction (OPIELIŃSKI, 2011). However, it allows precise determination of the size of heterogeneous areas > 9 mm, as visible in Fig. 11a,d,g (two boundary peaks inside), and a little less precise lesion areas in the size range $5 \div 9$ mm (start and end of one peak inside), as visible in Fig. 11b,c,f. An evaluation of sizes is possible for inclusions' areas < 5 mm (Fig. 11e).

The image of the distribution of attenuation coefficient can be treated as a quantitatively qualitative one, an image that indirectly visualises continuous and stepped changes (Fig. 6c,f). This image is a perfect complement of the images of velocity and the derivative of ultrasound attenuation, as it makes it possible to anticipate which of the visible heterogeneous areas are located in the horizontal plane that cuts across the centre of the surface of the sending and receiving transducer and which are outside of it (Fig. 13). The radiating surface of elementary ultrasonic transducers of the ring probe have to be narrow and high, due to the required high effectiveness and sensitivity, as well as the ability of high scanning resolution. It also makes it possible to achieve a beam that is wide horizontally and narrow vertically. Unfortunately, considerable height of the transducers (several mm) causes the imaged tissue cross-section to be averaged to the transducer's height.
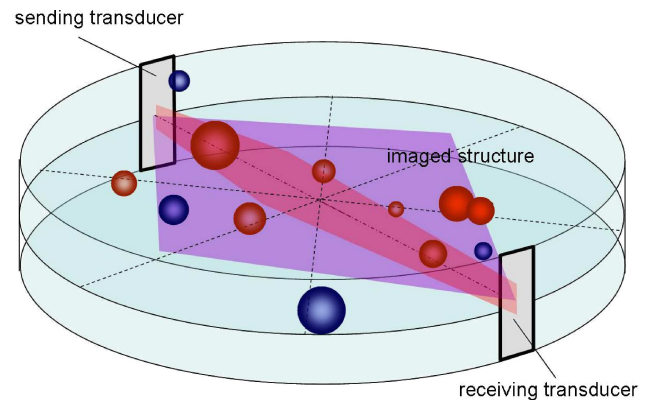

Fig. 13. Exemplary representation of the location of inclusions in the examined structure for the measurement space whose height is equal to the height of the elementary ultrasonic transducers of a ring probe (red inclusions are located in the horizontal plane of the transducer's axis).

As a result, the cross-section image shows structures that are slightly below and above the horizontal plane of the transducer's axis: there are 7 visible inclusions in the CT image (Fig. 8), and 10 in the UTT images (Fig. 6). As a result of a significant diversification of values of the attenuation coefficient inside inclusions, in comparison to the background (Fig. 11), the image of the distribution of local values of the ultrasound attenuation coefficient makes it possible, with increased contrast, to identify structures located

only in the studied cross-section with a high likelihood (Fig. 14). However, in a real breast tissue examination, a lesion located in the imaging plan can give less attenuation that another lesion, not located within the plane but with a higher attenuation coefficient. In that case, a contrast boost method can eliminate the on-plane lesion, which should be found on images of other kinds (attenuation derivative and velocity image) or on another cross-section image (close to the contrasted one).
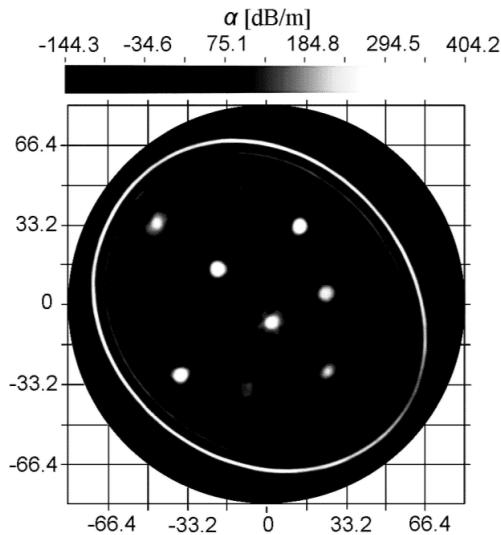

Fig. 14. UTT image of the distribution of local values of the ultrasound attenuation coefficient for the CIRS Model 059 phantom longitudinal cross-section for the height of $z = 20$ mm, with boosted contrast ($50 \rightarrow 90\%$) and reduced brightness ($50 \rightarrow 43\%$).

Lateral resolution of the UTT method (horizontal plane scanning density) primarily depends on ring probe's resolution (the number, width, and spacing of the elementary transducers), most of all. In the case of the 1024-element probe with 0.5 mm wide elementary transducers located 0.2 mm apart used in this study, the lateral resolution can be estimated to be in the range of 0.3÷0.4 mm, after transformation to the Cartesian coordinate system (1):

$$\Delta r_l = R_{\text{probe}} \cdot \sin\left(\frac{\pi}{N_{\text{probe}}}\right),\qquad(1)$$

where Δr_l – lateral resolution, R_{probe} – inner radius of a ring ultrasonic probe, N_{probe} – number of elementary transducers in a ring probe. Lateral resolution should not be lower than longitudinal resolution.

In the ultrasonic echo method the longitudinal resolution (axial, along the path of the wave beam) is often optimistically assumed to be half of the wavelength (DURIC *et al.*, 2007). In real measurements it should rather be assumed that this resolution is derived from the length (duration) of a received pulse, converted to distance in relation to the assumed ultrasound wave

velocity in the measured structure (NOWICKI, 2010). For the ultrasound frequency $f = 2$ MHz and single cycle length of pulse in a tissue, longitudinal resolution of the UTT method, determining sharpening in a tomographic image of the borders of the detected heterogeneous areas, can be estimated to be 0.77 mm. In reality it should be slightly better, as the structures that are smaller than the wavelength may be visible in an image as a result of diffraction – ultrasonic wave flows around a structure which, for example, means that the measured runtime is longer (OPIELIŃSKI, GUDRA, 2008). In such a case, however, information on the internal structure is distorted. Longitudinal and lateral resolution is additionally limited depending on the difference between the value of the acoustic parameter inside a heterogeneous structure and outside of it, as well as on the size of the structure. It is, therefore, possible to identify a heterogeneous area in an UTT image on condition that the average value of the acoustic parameter (measured on the path of ultrasonic wave beam from the transmitter to the receiver for directions around the heterogeneous area) is different from that value for the surrounding to a degree that can be measured. Additionally, the size of a heterogeneous area should not be lower than the scanning resolution and received pulse duration converted to distance. In other words, UTT contrast resolution affects spatial resolution and vice versa. It is also dependent on the examined structure. Longitudinal resolution can be improved by increasing ultrasonic wave frequency (although, attenuation inside a breast is a limiting factor) and by decreasing the Q-factor of the ultrasonic transducers (this leads to increased bandwidth and shortened pulse but also reduced effectiveness).

Vertical (elevation) resolution (in height) primarily depends on the vertical scanning density (layer thickness), with a limitation resulting from the transducer's height. If known simple equations are used (NOWICKI, 2010), it is possible, for the 1024-element ring probe with 18 mm high elementary transducers, to estimate the vertical resolution to be around 5 mm for the distance of 60 mm from the transducer (2):

$$\Delta r_v = \lambda \frac{2r}{h_t},\qquad(2)$$

where Δr_v is the vertical resolution, λ is the wave length, r is the distance from the transducer of a probe, h_t is the height of the elementary transducer of a probe. This, however, is not a significant limitation for the UTT method because there are ways to focus the beam vertically and consequently to increase elevation resolution. One of the ways is to use a lens on the surface of the transducers of the ring probe in the form of a suitably shaped layer. Ultrasonic concave lenses are made of elastic materials, e.g. plexiglass ($c \approx 2700$ m/s) or epoxy resin ($c \approx 2750$ m/s), while convex lenses are

made of silicone based materials, whose ultrasound velocity is below 1500 m/s. It is also possible to use transducers whose surface is shaped as a concave sphere. Another method is to make a horizontal incision (or a cut) in the radiated surfaces of elementary transducers and divide them into several lines (3 or 5) which make it possible to focus on using the electronic delay along their height (so called 1.5-D arrays) (NOWICKI, 2010).

4.3. US

Ultrasonography (US) is one of the methods of diagnostic breast imaging that is routinely used as the first or complementary test in relation to roentgen mammography (BASSET *et al.*, 2005). For example, the method allows to distinguish cysts from solid lesions, it is useful for precise determination of the location of a breast lesion, especially before a planned fine-needle biopsy and in young women, whose breast tissue is typically too dense for diagnostically reliable roentgen mammography. Ultrasonic probes with 5÷10, 5÷12 MHz range variable frequencies are mostly used in breast US diagnostics. Thus, US detects breast microcalcifications and, most importantly, makes it possible to assess lesion vascularity (abundance of blood vessels is typical of malignant and inflammatory lesions). However, it is a qualitative type of imaging which only allows visualisation of heterogeneity borders (WRONKOWSKI, ZWIERNO, 2000). Reflections of ultrasonic wave pulses from microcalcifications allow for signals received by the US-scanner to be obtained. This, however, does not mean that such signals will always be distinguishable in an US image from many other signals received from the border of the adipose, fibrous, glandular tissue, and their heterogeneity (tissue noise) (FILIPCZYŃSKI, 1983). The use of US scanners with Doppler method allows for lesion vascularity to be assessed. However, this method does not make it possible to distinguish unequivocally malignant lesions from benign ones. Additionally, US imaging produces a limited viewing area, it is subjective (depends on the examining person's assessment) and generates results that are an effect of a compromise between the ultrasonic wave penetration depth and image resolution (a higher frequency of the ultrasonic wave increases resolution but also attenuation and, as a result, it decreases the penetration depth). Imaging fidelity of an US image is dramatically affected by the width and frequency of the ultrasonic beam and scanning pulse length. The probability of early breast cancer detection using US is estimated to be about 50% (WRONKOWSKI, ZWIERNO, 2000).

None of the US images of the examined CIRS Model 059 phantom cross-sections revealed the heterogeneity of its structure. The differentiating parameter in ultrasonography is acoustic impedance, which means that the difference of its value between gel and inclusions structure is in this case too small and cannot be visualized.

4.4. Magnetic Resonance Imaging

MRI mammography (magnetic resonance imaging of women's breasts) is a method that makes it possible to detect even small areas in breasts that with high probability can be identified as early-stage neoplasm (BASSET *et al.*, 2005; PRUSZYŃSKI, 2000). However, it usually requires a contrast medium to be intravenously injected. If a patient receives a contrast agent, it is always possible that there could be an allergic reaction. This risk, however, is lower than in the case of contrast substances containing iodine that are typically used during roentgenography and computed tomography. No additional patient health hazards have been found in MRI. Since the examination exposes patient to a strong magnetic field, it is contraindicated for those patients that have (ferromagnetic) metal instruments or implants. Magnetic resonance imaging visualizes concentration of nuclei of hydrogen atoms (protons) (PRUSZYŃSKI, 2000). The largest number of protons can be found in water molecules. Water is the basic component of tissues but proportions in relation to other chemical compounds varies. This results in observable changes of signals in resonance emission caused by hydrogen atoms present in water molecules in tissues. Magnetic resonance imaging allows chemical analysis of biological media showing differences in water contents in comparison to other chemical compounds. As a result, MRI is the best type of examination for detecting diseases which cause an increase in fluid amount in the areas of pathological lesions caused by tumours, infections, and inflammations.

The quality of MRI images is significantly affected by the specifications of the measurement equipment (value of the magnet's induction, force of the gradients, receiving system, the coil used, etc.) and selection of the parameters of the scanning sequence (PRUSZYŃSKI, 2000). Seemingly unimportant changes in the basic imaging parameters can result in obtaining slightly different data which enable various diagnostic interpretations. MRI signal intensity depends on the used measurement sequence and, at the same time, on at least five tissue distinguishable factors: proton density ρ_p, longitudinal relaxation time (spin-lattice) T_1, transversal relaxation time (spin-spin) T_2, repetition time T_r, time of the echo T_e. By selecting specific T_e and T_r it is possible to emphasize the effect of individual tissue parameters in a signal; it is also possible to select such imaging parameters that the signal of a given substance will be muted (e.g. water, fat). If, for example, amplitude intensity of the nuclear magnetic resonance is primarily dependent on the density of protons, relaxation time effect will be reduced. Similarly, it is possible to create images dependent on times T_1 and T_2.

For short times T_e and T_r the image is dependent on time T_1 (water on the images is hypointense – black), and for long times T_e and T_r the image is dependent on time T_2 (water on the images is hyperintense – bright). Long times T_r and short times T_e make it possible to obtain an image dependent on the proton density. Water protons in malignant neoplasm tissue are usually characterised by longer relaxation times T_1 and T_2. In an image dependent on T_1, neoplasm tissue is darker, while in an image dependent on T_2 it is brighter that the surrounding area. The choice of T_r and T_e results from the need to achieve a maximum contrast between tissues. MRI images' resolution depends on the number of water protons, both free and as part of macromolecules, in a medium. The resolution of magnetic resonance imaging can be as high as about $0.4 \div 1$ mm. However, MRI tomographs are very expensive. Significant costs are also associated with their installation and maintenance, as it is necessary to service and calibrate them periodically.

MRI images of the studied CIRS Model 059 phantom clearly show inclusions in the structure. The sizes of the same inclusions estimated based on MRI images (Fig. 9) are different from those estimated based on CT images but this is caused by the difference between the tested cross-sections, as well as possible differences (mismatch) between the sizes of inclusions for the horizontal (CT) and vertical cross-sections (MRI). Another problem was related to the examination method (same as in the case of *in vivo* breast examination): the phantom was positioned in a special breast grip, at an angle, with the side parallel to the gantry hole (Fig. 5b). As a result, it is difficult to match and compare cross-sections with other imaging types. Additionally, the resolution of scanning of cross-sections of the phantom was just 5 mm (thickness of the layer). On the

other hand, the advantage of MRI images is additionally showing the diversification of the structures inside the inclusions (Fig. 9). The small black areas in the inclusion structure and phantom gel are air bubbles.

5. Conclusions

The comparison of resolutions of all imaging methods used in the paper is presented in Table 1. Additionally, the contrast values between an inclusion and the background in obtained images of the CIRS Model 059 breast phantom structure were evaluated, together with the average pixel value range variation in the background phantom gel (Table 1).

The obtained UTT, CT, and MRI images of the CIRS Model 059 breast phantom structure show comparable (in the context of size and location) heterogeneities inside it. On CT images they are hardly distinguished from the background, while on MRI images the distinction is fairly clear. The edges of inclusion in the phantom on CT and MRI images are sharp because of a high spatial resolution of those methods. US images are not suitable to identify any inclusions in any cross-section of that phantom.

Each of the 3 UTT images is characterised by slightly different features of the phantom's structure. The image of distribution of the ultrasound velocity clearly demonstrates continuous changes of density. The edges of small inclusions are fuzzy. It is a typical quantitative image, because of a high precision of digital determination of runtime. As a result, it is possible to identify the character of a breast lesion (benign or malignant (OPIELIŃSKI, 2011)) based on pixel values in the lesion area in relation to the background. The image of the derivative of the attenuation coefficient in relation to frequency is good for visualising edges and

Table 1. Comparison of resolutions and evaluated contrast values between an inclusion and the background in the CIRS Model 059 breast phantom structure images obtained by CT, UTT, US, and MRI.

Methods	Parameters			
	Spatial resolution [mm]	Layer thickness resolution [mm]	Longitudinal resolution [mm]	Contrast between an inclusion and the background imaging
CT	0.52	0.625	N/A	3 dB (3 dB range variation in the background)
UTT (velocity)	0.4	5	0.77 (2 MHz)	30 dB (3 dB range variation in the background)
UTT (attenuation derivative)	0.4	5	0.77 (2 MHz)	40 dB (4 dB range variation in the background)
UTT (attenuation)	0.4	5	0.77 (2 MHz)	40 dB (0.5 dB range variation in the background)
US	≤ 2.0 ≤ 1.5	2.9 2.5	0.44 (3.5 MHz) 0.31 (5 MHz)	0 dB – inclusions invisible (10 dB range variation in the background)
MRI	0.38	5	N/A	1.5 dB (0.5 dB range variation in the background)

bad for continuous changes. Since it distorts absolute values of the image pixels, it can be treated as more qualitative. The image of the distribution of attenuation coefficient can be treated as quantitatively qualitative. It visualises continuous and stepped changes in an indirect way. All the images show slightly different features of the structure and in this manner complement one another, providing important diagnostic information.

The obtained results show that, after the scanning process is accelerated making it possible to perform *in vivo* examinations (duration time of data acquisition, processing, and image reconstruction for one cross-section will be no longer than one second), the developed UTT method can successfully be used to detect and diagnose focal lesions in women's breasts (3-D whole breast imaging will take about 1.5 minute). Lesions that cannot be visualised using conventional US method can be imaged thanks to the UTT method. It combines the advantages of ultrasonography (no X-rays and contrast used, as well as no contraindications in the case of ferromagnetic implants) with transmission technology used in CT, making it an innovative (and most importantly) unusually sensitive "hybrid" method. The further developed prototype of a multimode ultrasonotomograph for *in vivo* examination of women's breasts will, apart from various 2-D and 3-D UTT images of the breast structure, reconstruct amplitude and phase URT images (ultrasound reflection tomography) (Stotzka *et al.*, 2002), combined US 2-D and 3-D images (Camacho *et al.*, 2012) and conventional US images that make it possible to view any part of a horizontal breast section in real time using a selected sector of a ring probe positioned at a given height.

Acknowledgments

References

1. Basset L.W., Jackson V.P., Fu K.L., Fu Y.S. (2005), *Diagnosis of Diseases of the Breast*, Elsevier Saunders, Philadelphia.

2. Camacho J., Medina L., Cruza J.F., Moreno J.M., Fritsch C. (2012), *Multimodal Ultrasonic Imaging for Breast Cancer Detection*, Archives of Acoustics, **37**, 3, 253–260.

3. Crawford C.R., Kak A.C. (1982), *Multipath artifact corrections in ultrasonic transmission tomography*, Ultrasonic Imaging, **4**, 234–266.

4. Duric N., Littrup P., Poulo L., Babkin A., Pevzner R., Holsapple E., Rama O., Glide C. (2007), *Detection of breast cancer with ultrasound tomography: First results with the Computed Ultrasound Risk Evaluation (CURE) prototype*, Medical Physics, **34**, 2, 773–785.

5. Ermert H., Keitmann O., Oppelt R., Granz B., Pesavento A., Vester M., Tillig B., Sander V. (2000), *A New Concept for a Real-Time Ultrasound Transmission Camera*, IEEE Ultrasonics Symp. Proc., 1611–1614.

6. Filipczyński L. (1983), *Detectability of calcifications in breast tissues by the ultrasonic echo method*, Archives of Acoustics, **8**, 3, 205–222.

7. Gudra T., Opieliński K.J. (2006), *The ultrasonic probe for the investigating of internal object structure by ultrasound transmission tomography*, Ultrasonics, **44**, 1–4, e295–e302.

8. Hoskins P.R. (2010), *Elastography Physics and Equipment* [in:] *Diagnostic Ultrasonud Physics and Equimpment*, Hoskins P.R., Martin K., Thrush A. [Eds.], Cambridge University Press, Cambridge, 196–214.

9. Kak A.C., Slaney M. (1988), *Principles of Computerized Tomographic Imaging*, IEEE Press, New York.

10. Nowicki A. (2010), *Ultrasound in medicine – introduction to modern ultrasonography* [in Polish], Wydawnictwo IPPT PAN, Warszawa.

11. Opieliński K.J., Gudra T. (2006), *Multi-parameter ultrasound transmission tomography of biological media*, Ultrasonics, **44**, 1–4, e295–e302.

12. Opieliński K., Gudra T. (2008), *Nondestructive tests of cylindrical steel samples using the ultrasonic projection method and the ultrasound transmission tomography method*, Acoustics '08, Paris, 4919–4924.

13. Opieliński K.J., Gudra T. (2010), *Ultrasonic Transmission Tomography* [in:] *Industrial and Biological Tomography*, Sikora J., Wójtowicz S. [Eds.], pp. 263–338, Wydawnictwo Książkowe Instytutu Elektrotechniki, Warszawa.

14. Opieliński K.J. (2011), *Application of transmission waves for characterization and imaging of biological media structures* [in Polish], Oficyna Wydawnicza PWr., Wrocław.

15. Opieliński K.J. (2012), *Ultrasonic Projection* [in:] *Ultrasonic Waves*, Antunes Dos Santos Júnior [Ed.], pp. 29–58, INTECH, Rijeka.

16. Pruszyński B. (2000), *Radiology, RTG, CT, USG, MRI Image Diagnostics and Radioisotopes* [in Polish], PZWL, Warszawa.

17. Quan Y., Huang L. (2007), *Sound-speed tomography using first-arrival transmission ultrasound for a ring array*, Proceedings of SPIE, **6513**, 651306-1-9.

18. Reguieg D., Padilla F., Defontaine M., Patat F., Laugier P. (2006), *Ultrasonic Transmission Device*